THE FILAMENTARY MULTI-POLAR PLANETARY NEBULA NGC 5189[1]

L. Sabin,[2] R. Vázquez,[2] J. A. López,[2] Ma. T. García-Díaz,[2] and G. Ramos-Larios[3]

RESUMEN

Presentamos un conjunto de imágenes ópticas e infrarrojas combinadas con espectros de rendija larga de mediana y alta dispersión de la Nebulosa Planetaria (NP) del sur NGC 5189. La compleja morfología de esta NP es desconcertante y no había sido estudiada en detalle hasta ahora. Nuestra investigación revela la presencia de un toroide denso y frío, en el infrarrojo, el cual probablemente generó uno de los dos flujos bipolares vistos en el óptico y podría, mediante un proceso de interacción, ser también responsable de la apariencia retorcida del toroide óptico. Los espectros de alta resolución del MES-AAT muestran claramente la presencia de nudos y estructuras filamentosas, así como tres burbujas en expansión. Nuestros hallazgos sugieren que NGC 5189 es una NP cuadrupolar con varios conjuntos de condensaciones simétricas en la cual la interacción de flujos determinó su compleja morfología.

ABSTRACT

We present a set of optical and infrared images combined with long-slit, medium and high dispersion spectra of the southern planetary nebula (PN) NGC 5189. The complex morphology of this PN is puzzling and has not been studied in detailed so far. Our investigation reveals the presence of a new dense and cold infrared torus (alongside the optical one) which probably generated one of the two optically seen bipolar outflows and which might be responsible for the twisted appearance of the optical torus via an interaction process. The high-resolution MES-AAT spectra clearly show the presence of filamentary and knotty structures as well as three expanding bubbles. Our findings therefore suggest that NGC 5189 is a quadrupolar nebula with multiple sets of symmetrical condensations in which the interaction of outflows has determined its complex morphology.

1. INTRODUCTION

NGC 5189 (PK 307-03°1, PN G307.2−03.4, He 2−94) belongs to a group of bipolar planetary nebulae that exhibit more than one bipolar structure. Examples of objects in this class are NGC 2440 (López et al. 1998), NGC 6302 (Meaburn et al. 2008), NGC 6309 (Vázquez et al. 2008, NGC 1514 (Aryal, Rajbahak, & Weinberger 2010) and NGC 6644 (Hsia

et al. 2010). These objects represent particularly interesting cases of study as they show morphological signatures of episodic mass outflows, most likely emerging from a precessing source. This type of phenomenon is receiving increasing attention in the literature, and is found not to be restricted to PNe with bipolar morphologies. The point symmetric IC 4634 (Guerrero et al. 2008) and the elliptical Fleming 1 (PN G290.5+07.9) (López, Meaburn, & Palmer 1993) are examples of objects that have been discussed under assumptions of episodic, symmetric outflows with a precessing symmetry axis. In the case of elliptical PNe, instead of multiple lobes one finds twisted strings of ansae and condensations delineating the presumed precession of the symmetry axis. Theoretical models like those of Soker & Livio

---

TABLE 1

PHYSICAL PROPERTIES OF NGC 5189 AND
ITS CENTRAL STAR

Property	Value
Type PN	I[a], IIa[b]
Distance (kpc)	0.88[c], 0.90[d], 0.55[e], 0.70[f], 0.54[l]
$c(H\beta)^{Balmer}$	0.65[a], 0.85[l]
$c(H\beta)^{Radio}$	0.56[a], 1.83[l]
S_ν(5 GHz) (mJy)	455[c], 507[l]
Θ_{diam} ($''$)	140[c], 163.4×108.2[j]
T_e([O III]) (10^4 K)	1.31 ± 0.05[a]
N_e([S II]) (cm^{-3})	390 ± 60[a], 200–900[i], 1000[l]
T_{eff} (K)	135×10^{3k}
Stellar Type	[WC 2][g], [WO I][h,i] (O VI seq.)
$\log (L_\star/L_\odot)$	2.9 ± 0.5[k]

References: [a]Kingsburgh & Barlow (1994), [b]Quireza, Rocha-Pinto, & Maciel (2007), [c]Zhang (1995), [d]Tajitsu & Tamura (1998), [e]Phillips (2004), [f]Maciel & Koppen (1994), [g]Mendez (1991), [h]Miszalski et al. (2009), [i]Polcaro et al. (1997), [j]Tylenda et al. (2003), [k]Althaus et al. (2010), [l]Hua, Dopita, & Martinis (1998).

(1989, 1994), based on close binary systems combined with a precessing systemic axis, describe one of the plausible scenarios under which such conditions may occur. The implication of magnetic fields should not be discarded as magnetohydrodynamic (MHD) models such as those by García-Segura et al. (1999) were able to reproduce the collimated outflows (or jets) observed, by coupling magnetized winds and stellar rotation.

Phillips & Reay (1983) have pointed out the interesting structure of NGC 5189 which they describe at first sight as "highly chaotic". In their electronographic narrow band images they identified five pairs of condensations or ansae (low-ionization structures following Gonçalves, Corradi, & Mampaso 2001) symmetrically distributed with respect to the central star (CS) at different position angles. The authors infer the occurrence of multiple mass loss events with a change of orientation in time to explain the observed pattern. And to account for the precessing phenomenon, they suggest the presence of a binary system (sheltering the precessing central star) with a few days period. To our knowledge no binary companion has been detected so far in NGC 5189.

Reay, Atherton, & Taylor (1984) used a wide field imaging Fabry-Pérot system to obtain a bidimensional line profile map of NGC 5189. By this mean they derived the kinematics of two potential pairs of ansae and their results indicate low to medium

velocities. Indeed, the first pair, which corresponds to the smallest and closest (to the CS) condensations as defined by Phillips & Reay (1983), is described as an inner ring with an expansion velocity of 25.3 km s^{-1} (radially, from the CS). The radial velocities of the second more distant pair of ansae to the CS following Phillips & Reay (1983) have been derived as $\sim |8|$ km s^{-1}.

Despite its significant asymmetry, NGC 5189 has not been extensively studied from a morphological point of view; the main information collected is gathered in Table 1. Also, in this paper we present unpublished optical imaging data, medium- and high resolution spectra as well as newly analyzed infrared images from the Midcourse Space Experiment (*MSX*; Price et al. 2001) and the recent Wide-field Infrared Survey Explorer (*WISE*; Wright et al. 2010) surveys. The combination of datasets will help us to analyze in detail the morphological structure of the PN.

2. OBSERVATIONS AND RESULTS

2.1. *Optical Imaging*

A set of images of NGC 5189 was obtained at Las Campanas Observatory (LCO, Chile) on the 1.0 m Swope telescope in May 1990, with a Texas Instruments (TI#1) CCD detector. The effective scale is 0.435 arcsec/pixel corresponding to a nominal field of 5.8 square arcmin. The interference filters were centered on Hα λ6563 ($\Delta\lambda \simeq 78$ Å), [O III] λ5007 ($\Delta\lambda \simeq 70$ Å), [S II] λ6724 ($\Delta\lambda \simeq 76$ Å) and He II 4686 ($\Delta\lambda \simeq 70$ Å) with exposure times of 600 s (Hα and [O III]), 900 s and 1200 s, respectively. The images, presented in Figure 1, were trimmed to 800×800 pixels and reduced with the standard IRAF[4] methods.

The [O III] frame (and to a lesser extent the He II one) in Figure 1 perfectly delineates the highly excited multiple outflows indicating the complex morphology, while the Hα+[N II] and [S II] frames underline the central part and borders of NGC 5189. Figure 2 presents the three likely outflows seen in NGC 5189 (well illustrated in the [O III] image) and numbered 1, 2, and 3, orientated at the respective position angles (PA) of 90°, 37° and 141° and the respective associated pairs of collimated outlows A1–A2, B1–B2 and C1–C2. The existence of a fourth outflow (numbered 4 on Figure 2) at PA 10° is less

---

[4]IRAF is distributed by the National Optical Astronomy Observatory, which is operated by the Association of Universities for Research in Astronomy (AURA) under cooperative agreement with the National Science Foundation.
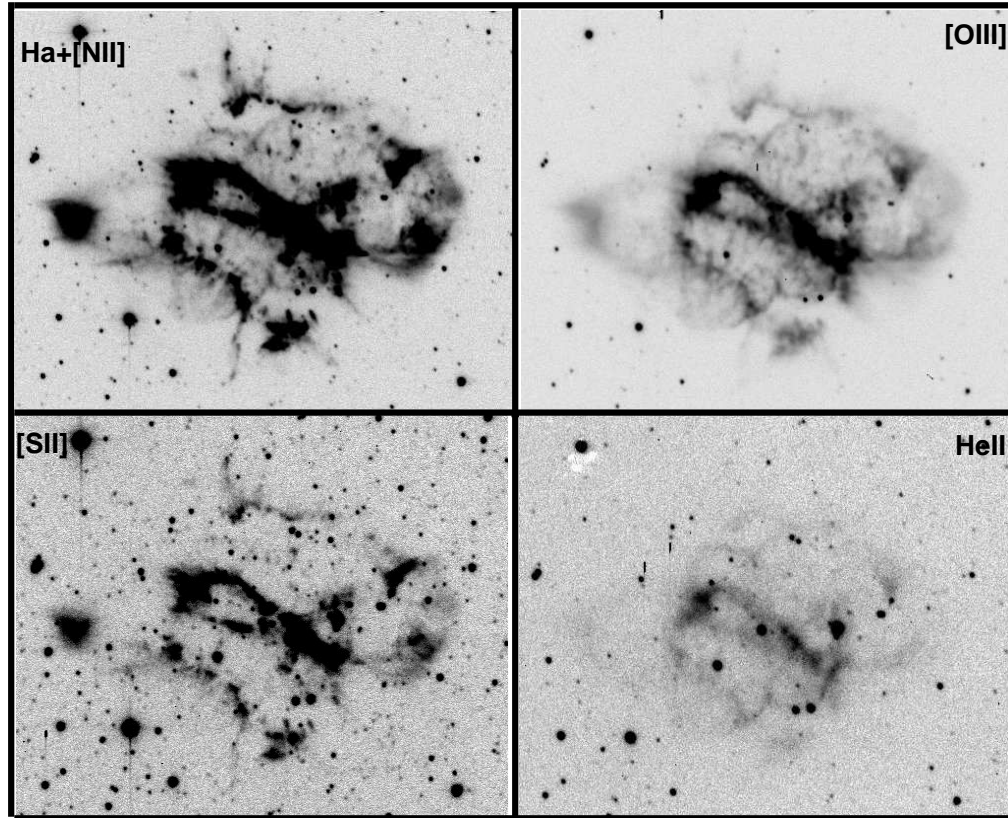
Fig. 1. Logarithmic scale images of NGC 5189 in Hα+[N II], [O III], [S II] and He II taken with the 1.0 m Swope telescope at LCO. North is up and east is left in a field of view of $\simeq 3.7 \times 3.0$.

clear, as only the 'polar' caps of the probable ejections are seen (D1 and D2). This case will be discussed later in the article. All the bipolar structures are emerging from the same geometric center related to the central star. The condensations or ansae defined by Phillips & Reay (1983) which include the opposite structures named B1, B2, and C by Reay et al. (1984) are clearly identified in our images (and particularly in the image ratio Hα(+[N II])/[O III], Figure 3) and correspond to the tips of the axes 1 and 4 (A2, D1, and D2). The Hα(+[N II])/[O III] frame, which traces the excitation conditions, also shows that the high excitation structures are mainly related to the central toroidal-like belt and the outer edges of NGC 5189. It is also interesting to notice from the image ratio in Figure 3 that the [O III] emission is globally enclosed in this Hα+[N II] 'nested bubble' and seems to form a bipolar structure whose waist is coincident with axis 4 and whose long axis is coincident with axis 1. The [S II] emission is distributed similarly to that of Hα+[N II] and from Figure 3 (top and bottom right), it appears that the string of knots forming the outer edges (the opposite

north-west and south-east rims), may in fact reflect a discontinuity in the high excitation outer shell of the PN. The poly-symmetric structure of NGC 5189 is clearly related to its dynamical evolution. A signature of this dynamical process are the dark lanes well seen in between knots of the south-east outer rim in the non-inverted Hα and [S II] images.

All images in Figure 1 clearly show the presence of a knotty central toroidal structure with a major axis size of about 78″ and a PA of $\sim 62°$. This structure seems flatter, tending more towards a disk description, with radial filaments emerging from its outer border. This torus/disk seems also to be slightly twisted. Several collimated cometary knots are located in NGC 5189 and are well seen in Figure 4. Those knots suggest the interaction of the stellar wind and photoionizing flux with the nebular material.

2.2. *IR imaging*

The dust and molecular content of PNe has often been used as a morphological tracer in the infrared wavebands (e.g., Phillips & Ramos-Larios
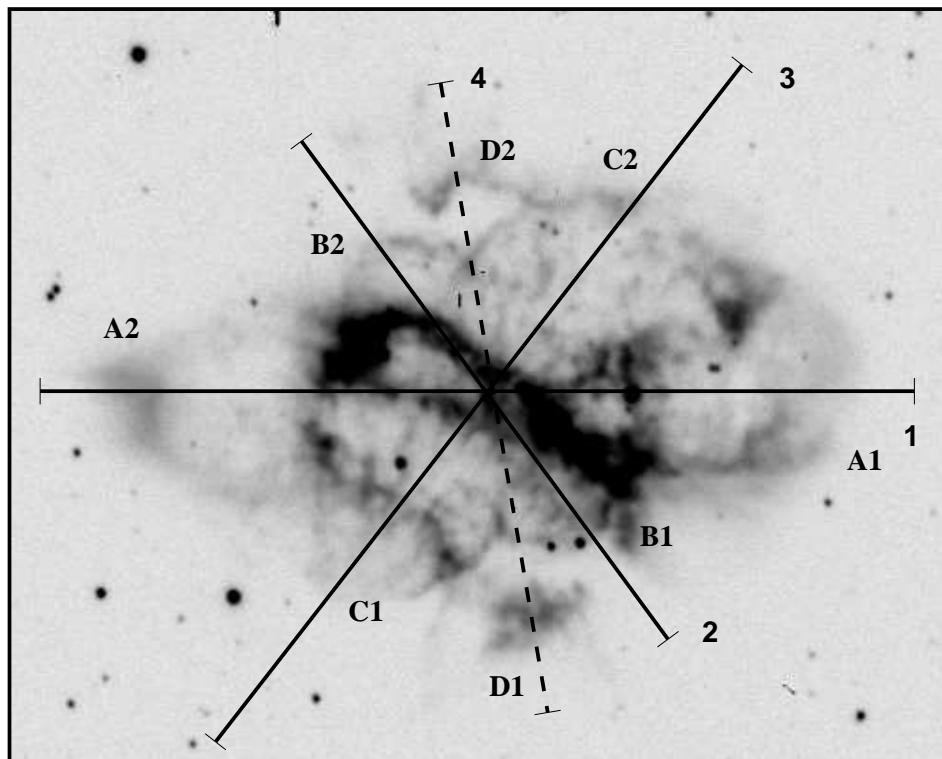
Fig. 2. Location of outflows in the PN NGC 5189. The dashed line indicates a possible fourth ejection axis.

2008; Ressler et al. 2010; Ramos-Larios, Guerrero, & Miranda 2008). We present Near-, Mid-Infrared (NIR and MIR) and H_2 images of NGC 5189. In Figure 5 we show the D-band (14.65 μm) image of the MIR *MSX* as well as a composite image of the data bands A, D, and E at the respective wavelengths 8.28 μm, 14.65 μm and 21.34 μm. The respective fluxes are 0.216 Jy at 8.28 μm, 1.029 Jy at 14.65 μm, and 1.635 Jy at 21.3 μm, with respective quality flux of 3, 2 and 1 (i.e., good, fair and limit; Egan et al. 2003). The spatial resolution of $\simeq 18\overset{''}{.}3$ of the Spatial Infrared Imaging Telescope, which gathered the MSX data, allows us to distinguish a dusty structure which is found to be coincident with the torus and some parts of the outer borders of the PN when compared to an optical image. From the *MSX* data, mainly the D band, it is clear that the dust is not uniformly distributed, with more material in the southern side of the toroid than in its northern side. But this effect could be due to the projection of the toroid.

WISE images, from the preliminary catalogue and image atlas, were retrieved from the NASA/IPAC Infrared Science Archive (IRSA). *WISE* is a NASA Explorer mission that surveys the entire sky at wavelengths of 3.4, 4.6, 12, and 22 μm

(W1 through W4, respectively). An advantage of *WISE* is its angular resolution, better than that of *MSX*, with $6\overset{''}{.}1$, $6\overset{''}{.}4$, $6\overset{''}{.}5$ and $12\overset{''}{.}0$ at 3.4, 4.6, 12, and 22 μm respectively.

Figure 6 (top-left) shows a 3-color image of NGC 5189 using the 3.4 μm (blue), 4.6 μm (green) and 12 μm (red) [close to the MSX D band] where we immediately notice a bright *X*-shaped structure which also seems to display much fainter ansae. The peculiar central morphology is well seen at the largest wavelengths, i.e., in the W3 and W4 wavebands (12 and 22 μm, where the derived magnitudes are the brightest, with 5.7 mag and 2.0 mag respectively), which allow us to measure an opening angle of $\simeq 59°$ between both arms which also have nearly the same length ($\simeq 70''$ for the arm A and $\simeq 73''$ for the arm B). By comparing the WISE and optical morphologies we can appreciate the dusty nature of NGC 5189 with the 12 μm (and 22 μm) emission perfectly covering the whole nebula and coinciding with its optical edges. While the arm A is fully coincident with the optical torus, the arm B does not show any obvious optical counterpart, i.e., there is no other visible optical torus.

Finally, in order to estimate the distribution of molecular material in NGC 5189 we have retrieved
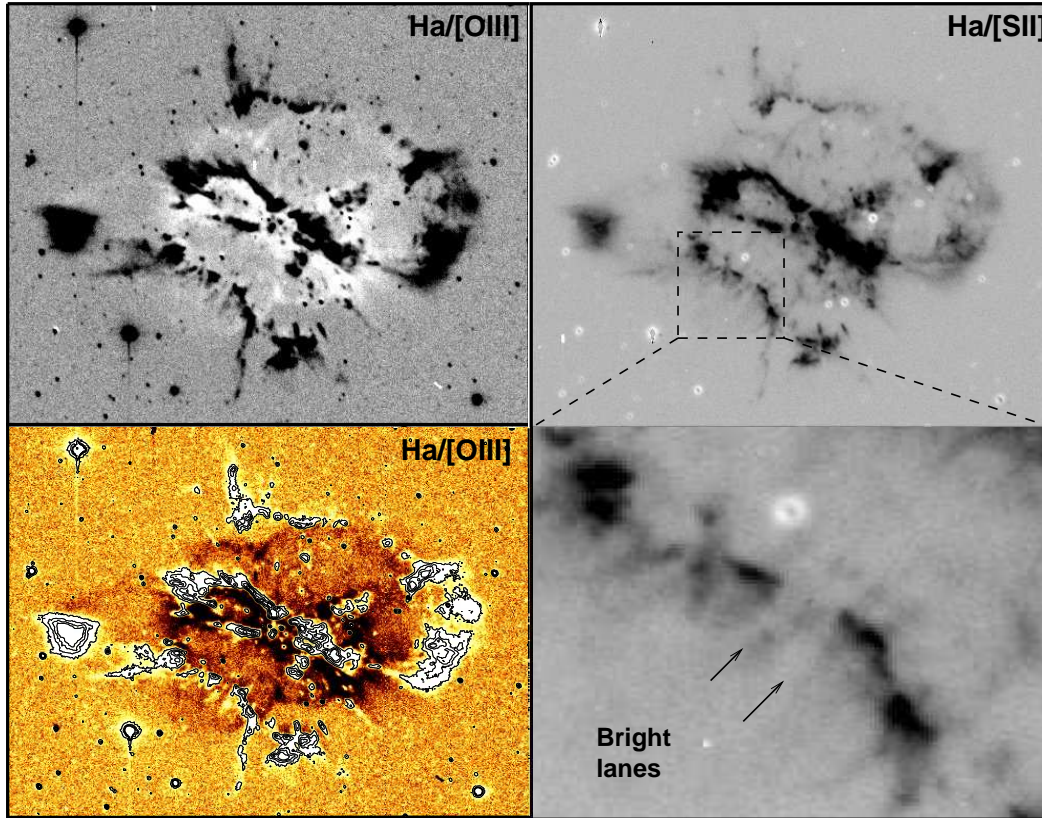
Fig. 3. Top: Image ratio using the Hα, [O III] and [S II] filters and a closer view of the knots alignment in the bottom right frame (zoom of top right frame). In each image ratio, black regions refer to high ratios, white regions refer to low ratios. Bottom left: Highlighted contours of the high excitation zones (condensations) in the Hα/[O III] image. The [O III] emission is mainly concentrated inside the Hα+[N II] nested bubble. Bottom right: Dark lanes which appear as bright paths in the inverted image. The color figure can be viewed online.

the H and K_s data from the 2MASS catalogue and followed the prescription by Ramos-Larios, Kemp, & Phillips (2006) to infer the H$_2$ distribution in the nebula. The resultant map is shown in Figure 6 (bottom left and right) which we compare to the optical (Hα+[N II]) image. The results indicate that the molecular emission is mainly concentrated in the optical torus and there is some indication that H$_2$ is also found in the nebula's edges and particularly at the locations of the northern and southern cometary knots. The latter is in agreement with the molecular H$_2$ content generally found in this kind of structures.

2.3. Kinematics

Longslit spectra were obtained with the modular spectrometer on the 2.5-m du Pont telescope at LCO in June 1990. The spectrometer was used with its 200-mm camera combined with a CRAF CCD 1024 × 1024 pixels, with 12 μm/pixel size. A 1200 lines/mm grating was used to cover the spectral range from $\simeq\lambda\lambda6290$–6805 Å. The instrumental combination yields a spectral resolution of $\simeq2$ FWHM in pixels (linear dispersion of 0.479 Å/pixel) and a spatial resolution along the slit of 0.292 arcsec/pixel. A slit width of 1″ and 149″ long was set. The spectra were flat-fielded and wavelength-calibrated against separate exposures of a quartz and neon arc, respectively. Two exposures were obtained, one of 1200 s along SE-NW axes and the other one of 1000 s, at the same position angle PA=329°, but shifted 36″6 to the west (Figure 7).

The medium resolution spectra allow us to visually distinguish variations in shape along each spectral line and velocity patterns. With a spectral dispersion of 0.479 Å/pixel over the spectral range yielding a resolution of 21.8 km s^{-1}/pixel, we were able to estimate the radial velocities along NGC 5189 at the two slits positions using the bright [N II] $\lambda6583$ line, adopting a rest wavelength $\lambda_{\rm lab} = 6583.454$ Å. The accuracy on the wavelength calibration is about

Fig. 4. Image of NGC 5189 processed with PixInsight underlining with unprecedented depth the detailed structures of the PN. The northern and southern caps (left and right bottom panels respectively) are maily composed of cometary knots. Credit: Juan Conejero with original raw data from the Gemini Science Archive (Hα: orange, [O III]: blue and [S II]: red). The color figure can be viewed online.
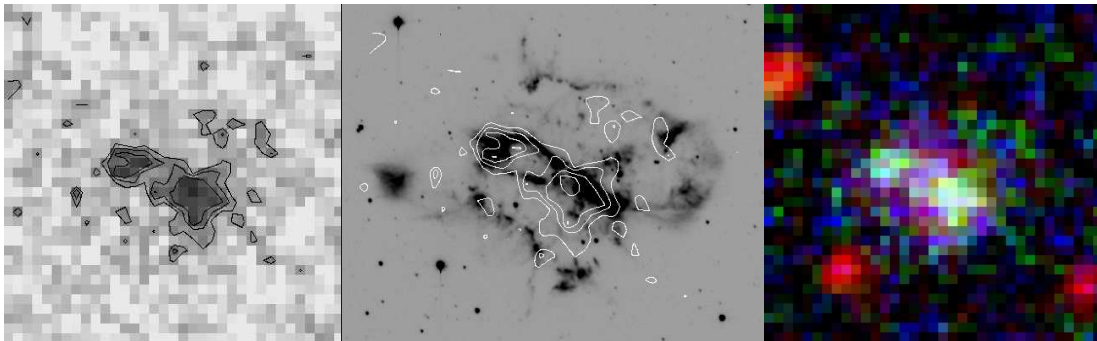

Fig. 5. From left to right (north is on the top and east on the left): (i) MSX 3.5 arcmin^2 IR image and contours of NGC 5189 in D band (14.65 μm). (ii) Contours of the MSX Band D emission overlaid on an optical image of NGC 5189. The IR emission matches the toroidal structure around the central star. (iii) Composite image of three MSX bands (A: red, D: green, and E: blue). The color figure can be viewed online.

4 km s^{-1}. As none of the slits pass through the location of the central star of the nebula, we cannot directly estimate the systemic velocity. However, this information was provided through our high resolution spectroscopy data (see below) which yielded a systemic velocity $V_{\rm lsr}$ of -13.3 ± 1 km s^{-1}. Fig-
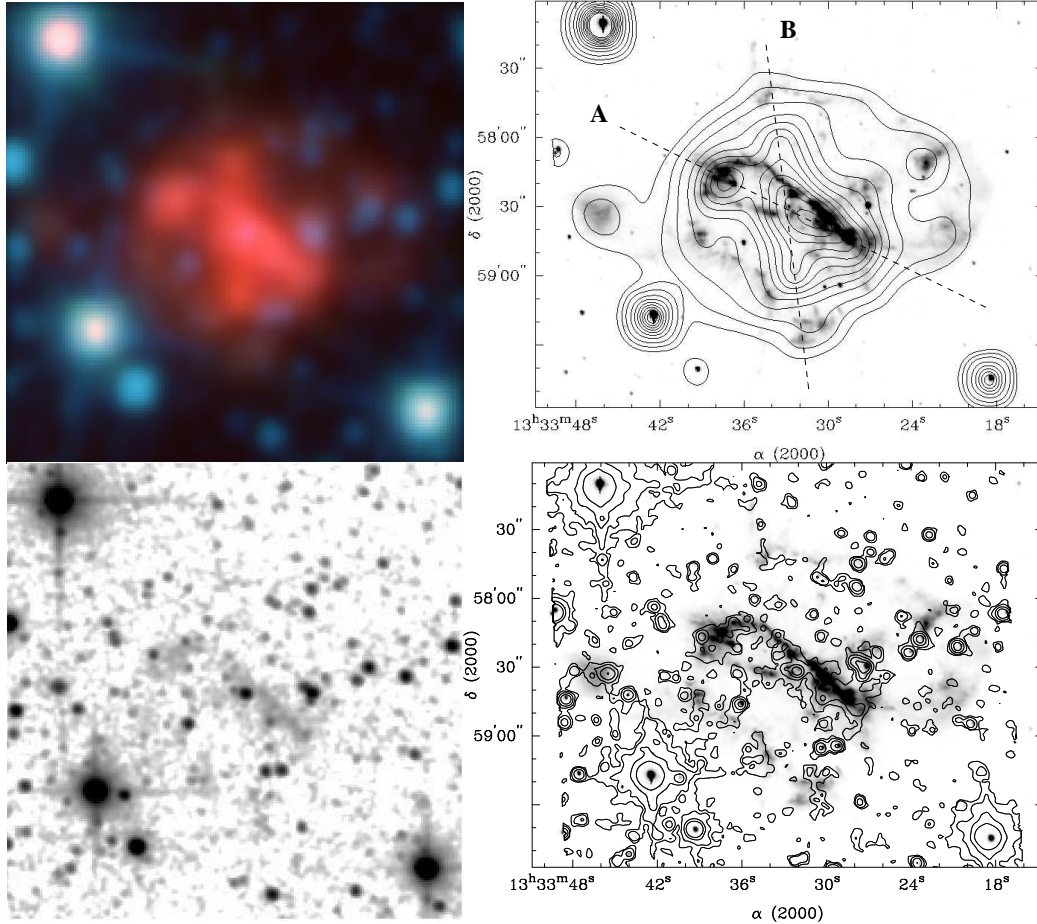
Fig. 6. Infrared imaging analysis of NGC 5189. Top left and right: Composite image of NGC 5189 using the 3.4 μm (blue), 4.6 μm (green) and 12 μm (red) and highlighting the central X-shaped structure. The contours of the 12 μm emission are overlaid on a Hα+[N II] image in the next image. Bottom left and right: H$_2$ map of NGC 5189 obtained with the 2MASS H and K_s broad bands. The contours overlaid on a Hα+[N II] indicate that the main optical torus is also emitting in molecular hydrogen. Other external structures such as the cometary knots and some parts of the edges are also emitting in this band. The color figure can be viewed online.

ure 7 shows the velocities at different points of the PN and although we only have the velocity pattern along the two slits, we can give an overall description of the kinematics considering NGC 5189 as a large butterfly-type (underlined by the external contours). Indeed, in accordance with Figure 7 it therefore appears that globally the northern part of the "optical" torus is blue-shifted (with negative values of -20 and -25 km s^{-1}) while the southern part is red-shifted (with mainly the positive velocity $+33$ km s^{-1}), giving us the orientation of inclination (Figure 8). And as one would expect (by a pure geometrical effect in an expanding axisymmetric nebula), the southern lobe of the butterfly envelope, is mainly blue shifted (Figure 7 indicates mainly negative velocities down to -44 km s^{-1}), while its northern counterpart is

red shifted (with a majority of positive values up to $+53$ km s^{-1}). The large scale kinematics of the nebula is in agreement with the results obtained by Reay et al. 1984).

In addition to the LCO spectra long-slit high resolution spectra, better suited for kinematic work, were obtained with the Manchester Echelle Spectrometer (MES; Meaburn et al. 1984) on the 3.9 m Anglo-Australian telescope (AAT). The observations, performed on 1997 April 14 with a Tektronix CCD with 1024×1024 rows of 24 μm square pixels, were obtained with a 100 Å wide filter containing Hα and the [N II] $\lambda\lambda6548$, 6584 Å emission lines. The spectral dispersion of $\simeq 0.05$ Å/pixel over the spectral range yielded a resolution of 11 km s^{-1}/pixel through a slit of width 150 μm. The total slit cov-
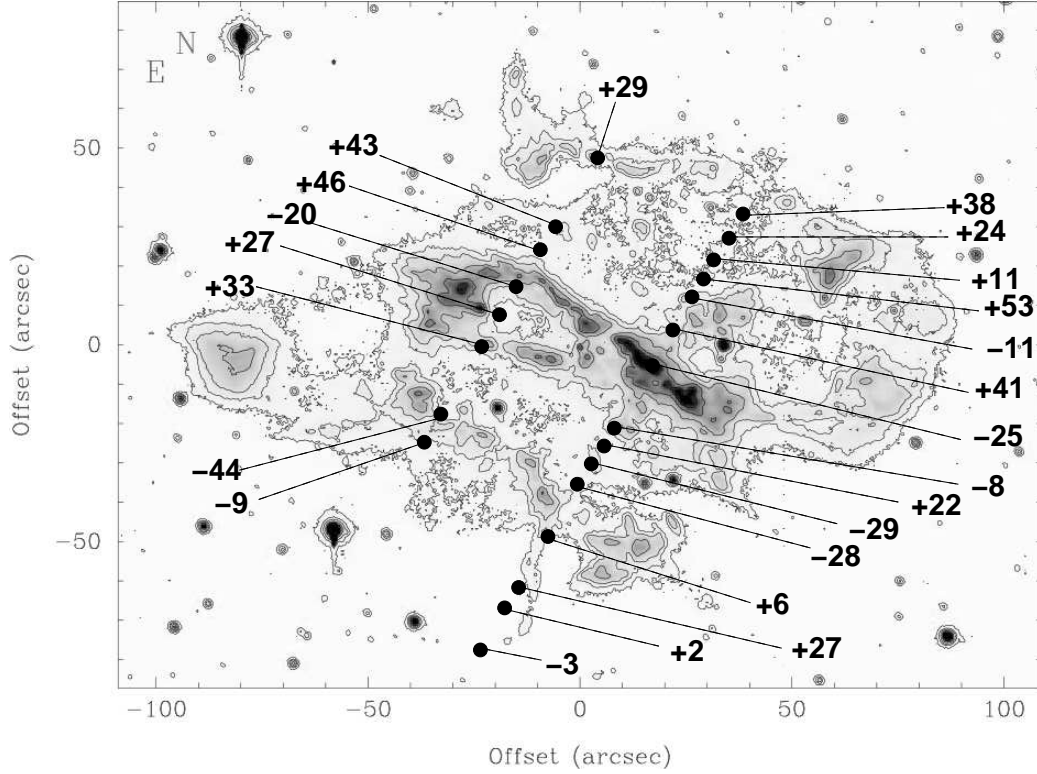
Fig. 7. Radial velocities along the LCO slits relative to the systemic velocity, with an accuracy of $\simeq 4$ km s^{-1}.

erage is composed of 3 exposures of 1200 s each, all at position angle PA=61°, and at opposite locations respective to the central star and the torus long axis (Figure 9). The CCD was binned by two in the spatial direction, giving $512 \times 0.32''$/pixel. These spectra are available in the *SPM Kinematic Catalogue of Galactic Planetary Nebulae*[5] (López et al. 2012). The structure of the line profiles, presented in Figure 10, is outstanding and reflects the highly filamentary and knotty structure of NGC 5189. Similarly to the LCO spectra, the different velocities obtained with the MES spectra were derived using the bright [N II] $\lambda 6584$ Å emission line. We identified a systemic velocity $V_{\rm lsr}$ of -13.3 ± 1 km s^{-1} ($V_{\rm hel} = -6.8 \pm 1$ km s^{-1}) which is comparable to the velocity derived by Schneider et al. (1983) within their error bar.

We also obtained the following maximum expansion velocities: $\Delta V = 35$ km s^{-1} in the north-west lobe (slit a), $\Delta V = 33$ km s^{-1} in the central region (slit b) and $\Delta V = 44$ km s^{-1} in the south-east lobe (slit c). Interestingly, these velocities do not show extreme values as would suggest the complex morphology.

[5]http://kincatpn.astrosen.unam.mx.

TABLE 2

VELOCITY POINTS FROM THE AAT-MES SPECTRAL DATA[a]

Slit A	$V_{\rm lsr}$	Slit B	$V_{\rm lsr}$	Slit C	$V_{\rm lsr}$
A1	+27	B1	+32	C1	−28
A2	+40	B1'	−34	C2	−27
A2'	−26	B2	−20	C2'	+13
AA	+11	B2'	+27	CA	−35
AB	−5	BA	−12	CB	−46
AB'	+14	BB	−13	CC	−10
AC	+52				
AD	+26				

[a]Calculated with a LSR corrected systemic velocity of -13.3 km s^{-1} and the spectral emission line [N II] $\lambda 6583.454$ Å. The error on the measurement is $\simeq 1$ km s^{-1}.

The data points with (') indicate a zone of expansion and correspond to the velocities measured using the faintest part of this expansion.

The MES-AAT spectra are positioned at $\simeq 92°$ with respect to those of the LCO and provide the same global kinematic information related to the
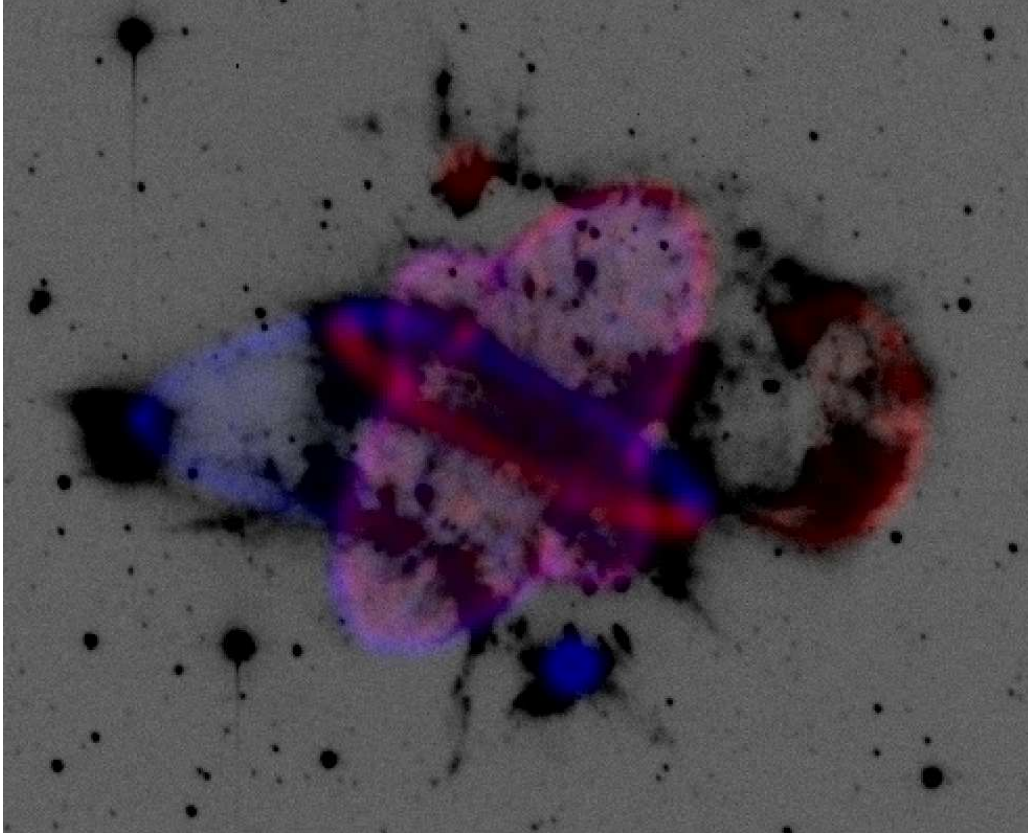
Fig. 8. Global kinemetical evolution of NGC 5189 based on the velocity measurements from the LCO and MES spectra. The blue components are blue-shifted and the red ones are red-shifted. The "model" was realized using the morpho-kinematical tool Shape (Steffen & López 2006). The color figure can be viewed online.

evolution of the main structures, as it can be seen in Figure 8. Figure 9 presents the detailed kinematics of several zones within NGC 5189 (cf. Table 2). The velocities of the structures belonging to the central torus at opposite sides (points BA and BB) evolve at pretty much the same rate with relative V_{lsr} values of -12 and -13 km s^{-1} respectively, similar to the systemic velocity. The torus is moving homogeneously towards us and therefore would not have the "warped" characteristics where one would expect to see an equally strong red-shifted side. The higher velocities at the expanding points B1 ($+32$ km s^{-1} and -34 km s^{-1}) and B2 (-20 km s^{-1}, $+27$ km s^{-1}) could be the result of the dynamic motions of structures which come across the torus. The cometary knots in the northern and southern parts of the nebulae (points AA and CC respectively aligned with axis 4 in Figure 2) show roughly the same velocities with $+11$ and -10 km s^{-1} respectively. Finally, the zones of NGC 5189 located on the [N II] rich butterfly edges (see Figure 3 top-left) have been studied (points CA, CB and C1 on the south-east and A1,

AC and AD on the north-west) and they globally show the same larger velocities. Thus, the mean velocity of the components of the "southern lobe" is $\simeq-36$ km s^{-1} while the mean velocity of the components of the "northern lobe" is $\simeq+35$ km s^{-1}.

3. DISCUSSION AND CONCLUSION

A detailed study of the seemingly complex structure of NGC 5189 has revealed a poly-polar morphology. The main findings are discussed below.

- This work highlights the presence of a new dense and cold infrared torus whose coincidence with the waist seen in the axis 4 in Figure 2 indicates that it gave birth to a bipolar outflow which coincides with the nested bubble of [O III] emission. The interaction of this newly discovered IR torus and the optical one (which are related to the same geometric center) might explain the warped morphology of the latter. The twisted torus hypothesis is ruled out by the kinematic measurements.
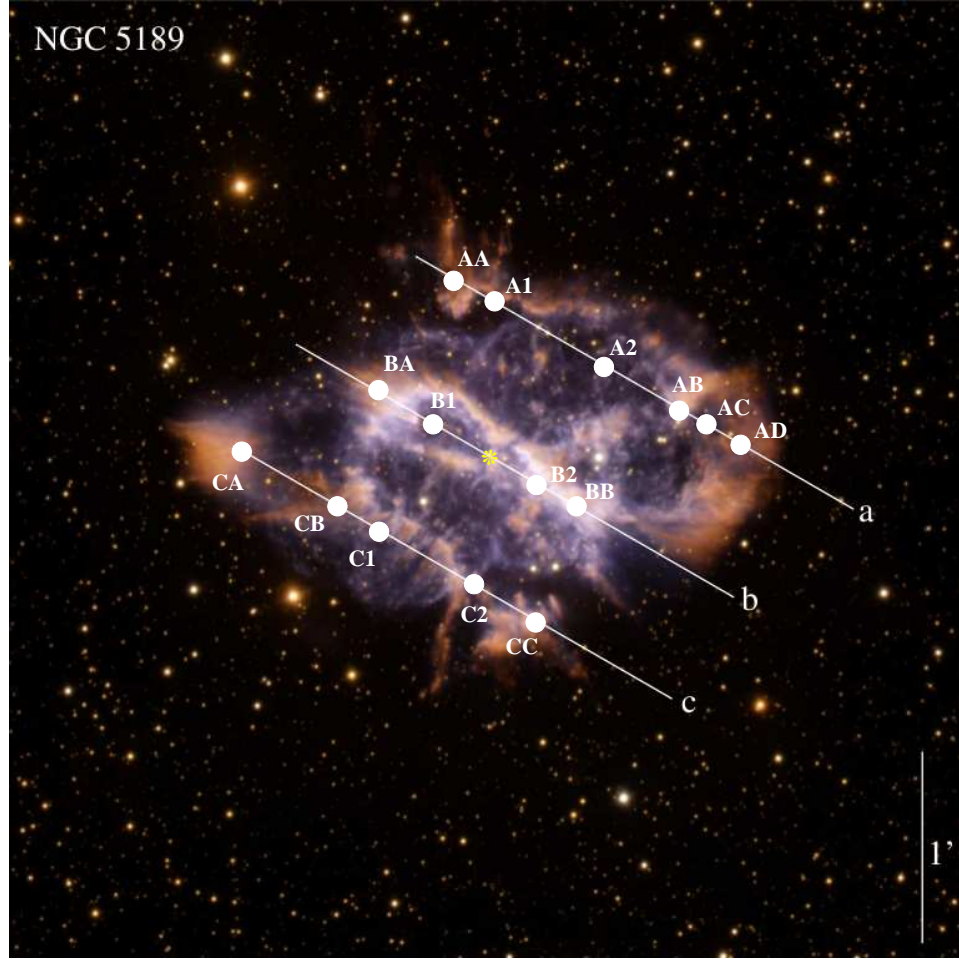
Fig. 9. AAT-MES slit positions superimposed on a $5' \times 5'$ composite GMOS image (H-α: orange, [O III]: blue and [S II]: red) from the Gemini South Observatory. North is up, east is left. The white dots indicate the areas where were derived the LSR corrected velocities: with A1, A2, B1, B2, C1 and C2 roughly corresponding to coinciding zones between the LCO and MES slits and the remaining points indicating the velocities of structures of interest, such as the cometary knots (cf. text and Table 2). The yellow star shows the central star location. The color figure can be viewed online.

- The MES-AAT spectra indicate the presence of filamentary and knotty structures as well as the expansion of three bubbles with the following velocities: $\Delta V = 35$ km s^{-1} in the north-west lobe (slit a), $\Delta V = 33$ km s^{-1} in the central region (slit b) and $\Delta V = 44$ km s^{-1} in the south-east lobe (slit c).

- The high resolution spectroscopy data also show that the largest velocities are found at both extremes of the nebula with -35 km s^{-1} and -46 km s^{-1} for the points CA and CB respectively on the eastern side of the PN (Figure 9), and $+26$ km s^{-1} and $+52$ km s^{-1} for the opposite points AD and AC on the western side. The similar velocities of the diametrically opposed

structures named AA and CC ($+11$ km s^{-1} and -10 km s^{-1}) seem to indicate that both are related.

We therefore suggest that NGC 5189 is structured along two symmetry axis each of them composed of a torus associated to a bipolar outflow. This corresponds to the IR torus combined to the [O III] bipolar emission which encloses the outflows B1–B2, C1–C2 and part of A1–A2 (see Figures 2 and 4); and the optical torus combined to the bright outer filamentary/knotty butterfly structure whose contours are well seen in the Hα/[O III] image ratio in Figure 3. Any other lobes would be the result of the expansion or dynamical motions of the existing nebular material in low-density or empty spaces.
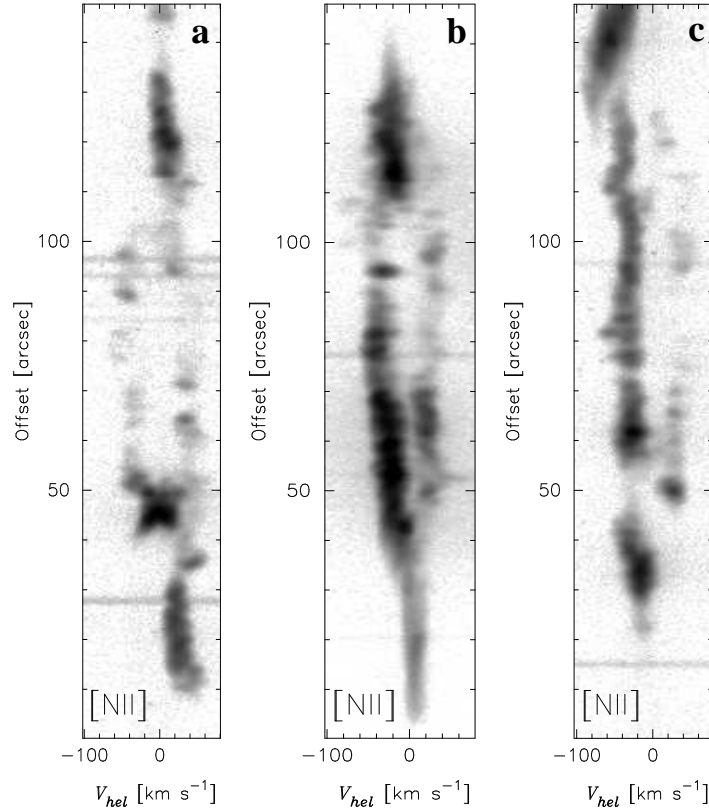
Fig. 10. AAT-MES [N II] $\lambda6583.454$ Å slit details underlying the filamentary structure of NGC 5189.

The combination of the imaging and spectroscopic data allowed us to make a first step in disentangling and (re-)defining the exact morphology of NGC 5189. Indeed, the "chaotic" aspect of NGC 5189 is the consequence of the encounter between two sets of bipolar outflows. The boundary between the different outflows is, however, not well determined with our kinematic data, although we can see it in the morphology, nor is the process leading to such evolution of the planetary nebula. We therefore need a more complete kinematical mapping (e.g., to derive the inclination angles and the kinematical ages of each structures) to have a better understanding of the formation of NGC 5189.

REFERENCES

Althaus, L. G., Córsico, A. H., Isern, J., & García-Berro, E. 2010, A&AR, 18, 471

Aryal, B., Rajbahak, C., & Weinberger, R. 2010, MNRAS, 402, 1307

Egan, M. P., et al. 2003, VizieR Online Data Catalog, 5114, 0

García-Segura, G., Langer, N., Rózyczka, M., & Franco, J. 1999, ApJ, 517, 767

Gonçalves, D. R., Corradi, R. L. M., & Mampaso, A. 2001, ApJ, 547, 302

Guerrero, M. A., et al. 2008, ApJ, 683, 272

Hsia, C.-H., Kwok, S., Zhang, Y., Koning, N., & Volk, K. 2010, ApJ, 725, 173

Hua, C. T., Dopita, M. A., & Martinis, J. 1998, A&AS, 133, 361

Kingsburgh, R. L., & Barlow, M. J. 1994, MNRAS, 271, 257

López, J. A., Meaburn, J., Bryce, M., & Holloway, A. J. 1998, ApJ, 493, 803

López, J. A., Meaburn, J., & Palmer, J. W. 1993, ApJ, 415, L135

López, J. A., et al. 2012, RevMexAA, 48, 3

Maciel, W. J., & Koppen, J. 1994, A&A, 282, 436

Meaburn, J., Blundell, B., Carling, R., Gregory, D. F., Keir, D., & Wynne, C. G. 1984, MNRAS, 210, 463

Meaburn, J., Lloyd, M., Vaytet, N. M. H., & López, J. A. 2008, MNRAS, 385, 269

Mendez, R. H. 1991, in IAU Symp. 145, Evolution of Stars: the Photoespheric Abundance Connection, ed. G. Michaud & A. V. Tutukov (Dordrecht: Kluwer), 375

Miszalski, B., Acker, A., Parker, Q. A., & Moffat, A. F. J. 2009, A&A, 505, 249

Phillips, J. P. 2004, MNRAS, 353, 589

Phillips, J. P., & Ramos-Larios, G. 2008, MNRAS, 386, 995

Phillips, J. P., & Reay, N. K. 1983, A&A, 117, 33

Polcaro, V. F., Rossi, C., Viotti, R., & Norci, L. 1997, A&A, 318, 571

Price, S. D., Egan, M. P., Carey, S. J., Mizuno, D. R., & Kuchar, T. A. 2001, AJ, 121, 2819

Quireza, C., Rocha-Pinto, H. J., & Maciel, W. J. 2007, A&A, 475, 217

Ramos-Larios, G., Guerrero, M. A., & Miranda, L. F. 2008, AJ, 135, 1441

Ramos-Larios, G., Kemp, S. N., & Phillips, J. P. 2006, RevMexAA, 42, 131

Reay, N. K., Atherton, P. D., & Taylor, K. 1984, MN-RAS, 206, 71

Ressler, M. E., Cohen, M., Wachter, S., Hoard, D. W., Mainzer, A. K., & Wright, E. L. 2010, AJ, 140, 1882

Schneider, S. E., Terzian, Y., Purgathofer, A., & Perinotto, M. 1983, ApJS, 52, 399

Soker, N., & Livio, M. 1989, ApJ, 339, 268

_____. 1994, ApJ, 421, 219

Steffen, W., & López, J. A. 2006, RevMexAA, 42, 99

Tajitsu, A., & Tamura, S. 1998, AJ, 115, 1989

Tylenda, R., Siódmiak, N., Górny, S. K., Corradi, R. L. M., & Schwarz, H. E. 2003, A&A, 405, 627

Vázquez, R., Miranda, L. F., Olguín, L., Ayala, S., Torrelles, J. M., Contreras, M. E., & Guillén, P. F. 2008, A&A, 481, 107

Wright, E. L., et al. 2010, AJ, 140, 1868

Zhang, C. Y. 1995, ApJS, 98, 659

G. Ramos-Larios: Instituto de Astronomía y Meteorología, Departamento de Física, CUCEI, Universidad de Guadalajara, Av. Vallarta 2602, C.P. 44130, Guadalajara, Jal., Mexico (gerardo@astro.iam.udg.mx).

L. Sabin, R. Vázquez, J. A. López and Ma. T. García-Díaz: Instituto de Astronomía, Universidad Nacional Autónoma de México, Apdo. Postal 877, 22830 Ensenada B. C., Mexico (lsabin, vazquez, jal, tere@astrosen.unam.mx).